

Radius of curvature metrology for segmented mirrors

Dave Baiocchi and J. H. Burge

Optical Sciences Ctr./Univ. of Arizona, Tucson AZ

ABSTRACT

Future space and ground telescopes will have apertures that are increasingly larger in size. The primary mirrors for these telescopes will be so large that they cannot be fabricated, transported, and/or launched as a single entity. One solution is to build a large mirror out of smaller segments. The biggest challenge in fabricating segmented mirrors is matching the individual pieces so they form a single, continuous surface. This requirement means that the radii of curvature must all match. We present a technique for matching the relative radii of curvature for segmented mirrors, and we include an error analysis of this method.

Keywords: Telescopes, segmented mirrors, radius of curvature

1. INTRODUCTION

The next generation of ground and space telescopes will have apertures larger than 10 and 8 meters, respectively. One solution for building primary mirrors of this size is to use segmented mirrors. There are several advantages to building a segmented mirror, Figure 1. The biggest advantage is that large numbers of small segments can be fit together to make large (> 10 m) aperture mirrors.

There are already two Earth-based telescopes which utilize a segmented primary mirror. The W. M. Keck Observatory on Mauna Kea, HI, has two identical telescopes, and each has a 10 m primary comprised of 36 hexagonal segments. The Hobby-Eberly Telescope (HET) at the McDonald Observatory started operating earlier this year. The HET's primary is comprised of 91 segments that form a 11 by 10 m hexagon.^{1,2}

Further author information:

Send correspondence to DB: baiocchi@optics.arizona.edu

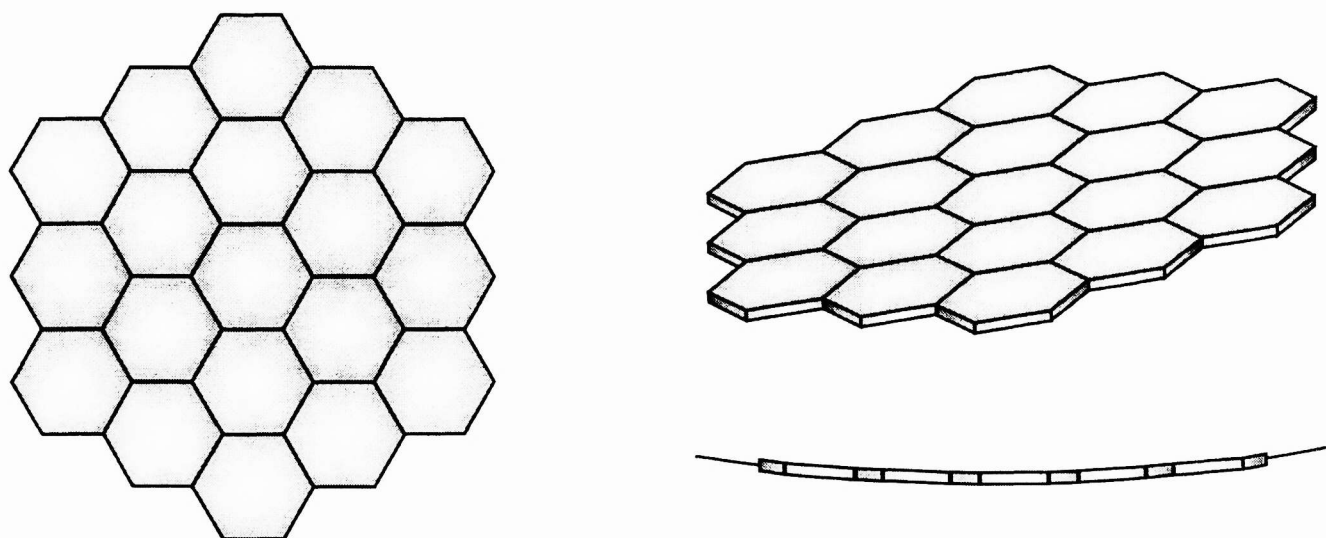


Figure 1. A segmented mirror. Lower right: For curved surfaces, each segment is fabricated so that it lies along a common curve.

For large space-based telescopes, a segmented primary is a necessity. Future space telescopes must be engineered so they comply with the size and mass restrictions imposed by the launch vehicle. A telescope can be launched into orbit in several small segments, and the final instrument can be assembled in space. There is also less risk in building smaller segments. If one of the segments is damaged, it can be easily replaced. If a monolithic mirror is damaged, the entire part must be recast.

The successor to the Hubble Space Telescope, the Next Generation Space Telescope (NGST), will have an 8 meter segmented primary mirror. While the most of NGST's details are still in the design phase, a segmented primary mirror will be part of the final telescope.

Until recent years, the Earth's atmosphere limited the resolution of Earth-based telescopes. Space telescopes are free from this limitation, and ground-based instruments are now utilizing adaptive optics to correct for the atmosphere. Due to these improvements all telescopes can now be designed to be diffraction-limited. A diffraction-limited instrument is one in which the resolution is no longer limited by the quality of the optics. Because of this, telescopes can now be built to optical tolerances, and it's crucial that the segments all have the same radius of curvature. We analyze the effect of radius mismatch on the system performance in Section 3.1.

The need to carefully match radii presents an interesting challenge for the optics shop. Measuring the radius of curvature (ROC) to a high level of accuracy using conventional tools is extremely difficult. In the following sections, we present a technique for measuring the relative radii of curvature of the mirror segments to within 10 microns.

2. METROLOGY

2.1. Test Setup for Radius of Curvature Measurements

For single, curved mirrors, measuring the radius of curvature is not of significant concern because it only introduces a defocus error. This defocus is easily removed by adjusting the position of one of the system elements. The optician uses conventional tools (a spherometer or inside micrometer), and measures the accuracy of the ROC to a few millimeters.

Multiple mirror systems combine several mirrors to form one large primary, and the errors *cannot* be corrected by moving the image plane. In order to minimize this error, the individual segments should lie along the same surface and have the same radius of curvature. It is therefore essential that the segments have their relative radii of curvature matched to within a few tens of microns.

Figure 2 shows our test plate setup for measuring the relative radii of the segments. The convex reference surface of the test plate should have a radius of curvature that is about 1 - 2 cm less than the mirror under test. The test plate is translated until all of the power is removed from the image. In doing this, we overlap the centers of curvature of the two surfaces. The gap between the facesheet and the test plate – which can be measured very accurately with a telescoping gauge and micrometer – represent the difference in radii between the test plate and the mirror surface. Additional segments are measured with a similar procedure: the test plate is translated to remove the power and the gap is measured. Note that this method is measuring the *relative* ROC between the mirrors, not the absolute radius.

An additional benefit of using this technique is that we can perform phase-shifting interferometry (PSI) with the setup. PSI is a powerful tool which creates a surface profile by varying the phase between the reference and test surface.³ This is done by physically moving the reference with respect to the test piece using piezo-electric transducers.

2.2. Test Setup for Radius of Curvature Measurements for Aspheres

All of the latest telescope designs use aspheric optics. Aspheres allow for a more efficient and compact optical design: light is collected more efficiently and the enclosure around the telescope is smaller.

The technique described in the previous section is easily modified into a scheme which measures aspheres accurately and efficiently. The technique⁴ employs a computer-generated hologram (CGH) that is projected directly onto the test plate.* A diagram of this scheme is shown in Figure 3. The test plate provides a reference surface, and the wavefront stored in the hologram is that of a perfect sphere. This wavefront is interfered with the reference beam's

*An alternative method is to write the CGH directly onto the test plate. However, this method requires a different test plate/CGH combination for every unique segment. For most applications, this technique is too costly to implement.

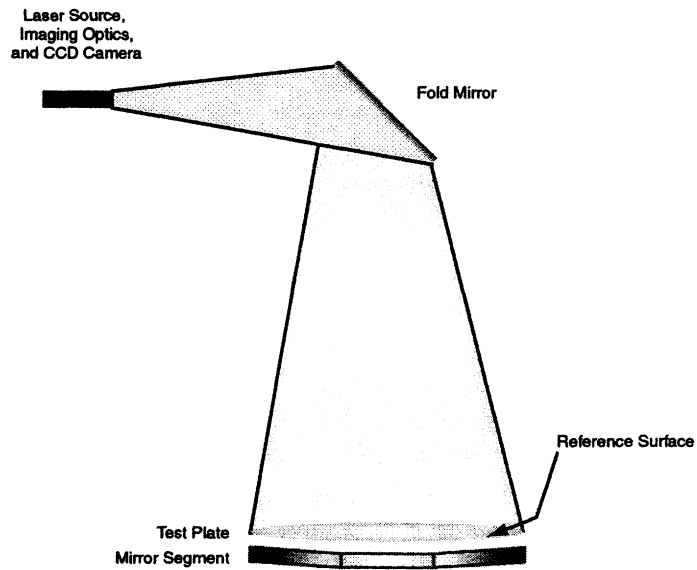


Figure 2. Test setup for ROC measurements.

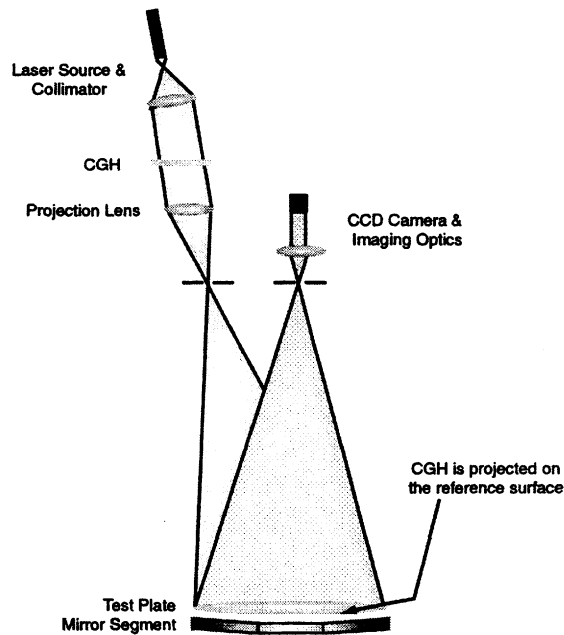


Figure 3. Diagram of the system which projects a CGH onto the test plate. The first two orders of diffraction from the CGH are projected onto the test part with a projection lens. The CGH is designed so the 1st-order light reflected from the segment will exactly match the 0-order light reflected from the test plate.

reflection off the test optic, and the resulting fringe pattern represents the residual error between the test part and ideal wavefront.

This system has several important advantages:

- High accuracy. Using holograms fabricated with electron beam lithography, this test can achieve an accuracy of $\frac{\lambda}{100}$ for large, steep, off-axis aspheres.

- Low cost. This test requires only one accurate surface: the reference side of the test plate.
- Accurate radius measurement. Using the technique described in Section 2.1, the relative radii of different segments can be measured to tens of microns.
- Efficient. For different off-axis segments, the only necessary modification is a new CGH. Thus, an entire system of segments is easily and quickly tested by simply inserting the appropriate CGH.

3. TEST ACCURACY

3.1. Radius of Curvature Error and System Performance

As we mentioned in Section 2.1, the ROC errors from the various segments cannot be removed at the image plane. Thus, for a segmented mirror, it is useful to determine how errors in the relative radii affect the system performance.

The Strehl ratio is a useful quantity for assessing the performance of a diffraction-limited optical system. A qualitative definition of the Strehl ratio is

$$\text{Strehl ratio} = \frac{\text{intensity of onaxis aberrated image}}{\text{intensity of perfect image}}.$$

For our system, we will determine how a typical error in the radius affects the Strehl ratio.

We begin by relating the error in the radius to the error in the sagitta:

$$S \approx \frac{D^2}{8R}, \quad (1)$$

where S is the sag, D is the segment diameter, and R is the ROC. We can take a derivative to see how errors in the ROC, ΔR , affect sag error:

$$\Delta S \approx -\frac{D^2}{8R^2} \Delta R.$$

We can define the segment “R-number” as $\frac{R}{D}$. This is more useful quantity than the F-number because mirrors are generally tested at their center of curvature. We can express the previous equation in terms of $R/\#$:

$$\Delta S = -\frac{1}{8} \frac{1}{(R/\#)^2} \Delta R. \quad (2)$$

Figure 4 shows a plot of Equation 2 for $R/7$, $R/10$, and $R/15$ optical systems. As expected, errors in the radius have a greater effect on the sag errors for “faster” (smaller R-number) systems. A low R-number means that the optic has a significant amount of curvature which quickly focus the incident rays.

Now that we have a relationship between radius error and sag error, we can describe the Strehl ratio in terms of ΔR . A convenient mathematical form for the Strehl ratio is

$$\text{SR} \approx e^{-(2\pi\sigma)^2} \approx 1 - (2\pi\sigma)^2, \quad (3)$$

where σ^2 is the wavefront variance in units of waves. The square root of σ^2 is the rms wavefront. This quantity is related to wavefront error as follows[†]:

$$\sigma = 0.289 W = 0.289(2 \Delta S). \quad (4)$$

We can substitute for ΔS with the expression from Equation 2:

[†]We derive the relationship between σ and W in Appendix A

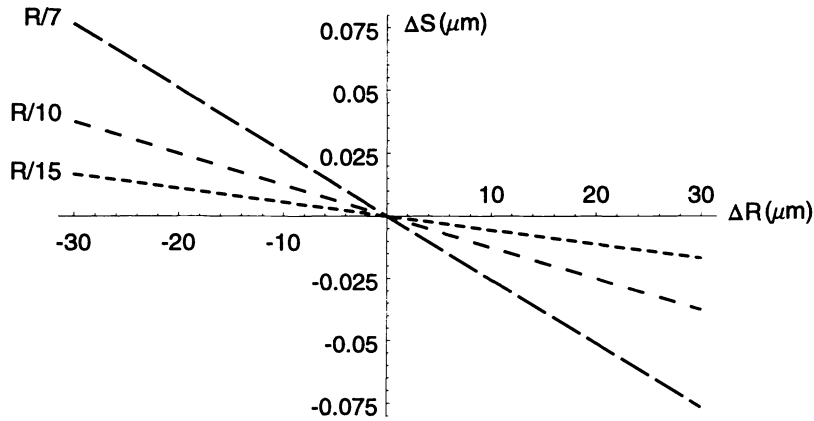


Figure 4. Plot of Equation 2. This effect is more severe for faster systems.

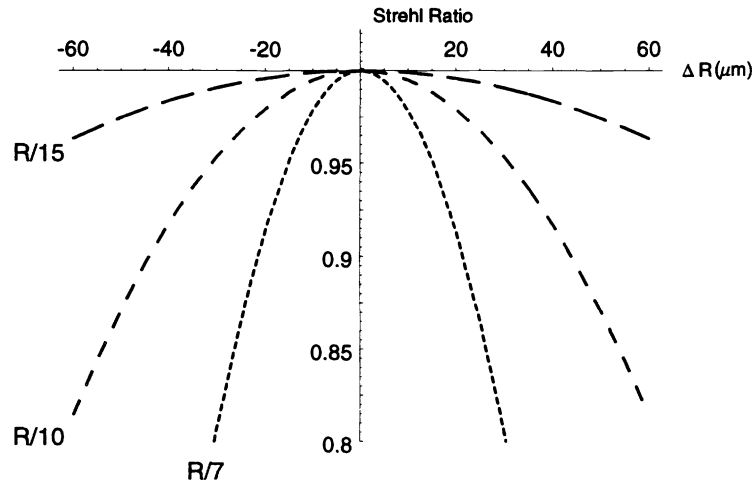


Figure 5. Strehl ratio as a function of ROC error. $\lambda = 633 \text{ nm}$ (HeNe).

$$\sigma = -0.289 \left(\frac{1}{4} \frac{1}{(R/\#)^2} \Delta R \right).$$

Finally, we'll put the previous result into the Strehl ratio, Equation 3:

$$SR \approx 1 - \left(-2\pi \cdot 0.072 \left(\frac{1}{(R/\#)^2} \frac{\Delta R}{\lambda} \right) \right)^2, \quad (5)$$

where we have used $\frac{\Delta R}{\lambda}$ so σ is in units of waves. Figure 5 shows a plot of Equation 5. Smaller R-numbers have a greater affect on the system performance.

3.2. Accuracy of the Relative Radius Measurement

There are three dominant sources of errors in the ROC measurement, and we now explain each in detail. These errors are summarized in Table 1.

The first error has to do with measuring the gap between the test plate and the facesheet. Because the gap represents the difference in radii between the two parts, errors in this measurement contribute directly as errors in radius measurement. A good telescoping gauge and micrometer can measure this distance to within 5 microns.

Another effect on the measurement accuracy depends on the ability to remove all of the optical power at the image. We can quantify this effect by recalling the relationship between sagitta (wavefront power) and segment diameter, Equation 1. Because we're actually interested in errors in the radius due to the sag error, we'll solve Equation 2 for ΔR :

$$\Delta R_{\text{power}} = -8 (R/\#)^2 \Delta S. \quad (6)$$

We now have an equation which relates residual sag, ΔS , to error in the radius measurement, ΔR .

Figure 6 shows a plot of Equation 6. The plot shows two separate curves. The dotted curve represents a ΔS of $\frac{\lambda}{8}$; this is a typical ΔS when an interferogram is used to remove the power to a quarter fringe. The solid curve represents a ΔS of $\frac{\lambda}{100}$. This is a typical value for ΔS when phase-shifting interferometry is used.

The final error is due to the fact that the light incident on the test plate is not perfect. As shown in Figure 7, this presents a problem because off-axis rays are not normal to the test surface. Along the optic axis, the light is normal to this surface, and it retraces the incident path back to the source. For off-axis rays, the light is not normal to the test surface, and this introduces an optical path difference (OPD) between the incident and reflected paths. We derive this error in Appendix B, and we'll simply state the results here. The error in the radius measurement due to this effect is

$$\Delta R_{\text{cos}} = -8 (R/\#)^2 d \cdot \alpha^2 \quad (7)$$

where d is the gap between the test and reference surfaces and α is the slope error in radians (deviation from normal incidence). This error is large for a large air gap, d . When designing this test, the engineer should specify a test plate such that the air gap is only a few centimeters.

We conclude with a simple example that illustrates each factor's relative contribution to the overall accuracy of the ROC measurement. We'll consider an R/10 segment; the results are shown in Table 2. Let's suppose that using good tools and techniques, we measure the physical gap with an accuracy of $\Delta R_{\text{gap}} = 5 \mu\text{m}$. Our setup allows us to remove all of the residual power except 31.6 nm ($\frac{\lambda}{20}$). We can use Equation 6 to calculate $\Delta R_{\text{power}} = -8 (10)^2 \cdot 31.6 \text{ nm} = -25.3 \mu\text{m}$. Finally, let's suppose that we have a 2 cm gap and a slope error of 0.001 radians. Using Equation 7 we find $\Delta R_{\text{cos}} = -8 (10)^2 (0.02\text{m})(0.001)^2 = -16 \mu\text{m}$. The RSS of these three values is

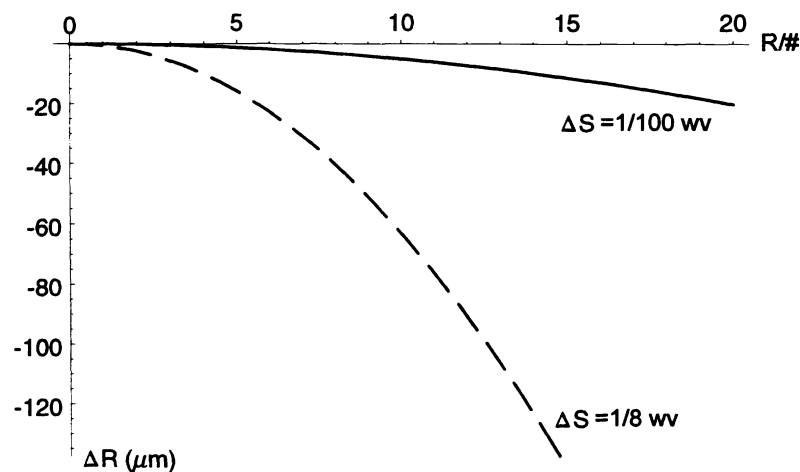


Figure 6. ΔR as a function of F-number. The dotted line represents a typical amount of residual power when an interferogram is used. The solid curve represents a PSI measurement. $\lambda = 633 \text{ nm}$ (HeNe).

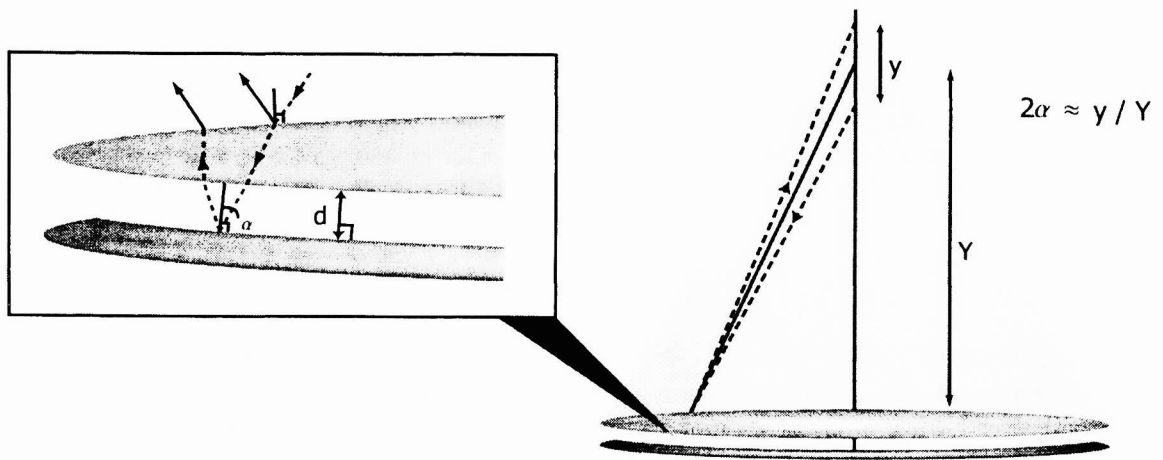


Figure 7. Right: Light incident near the edge of the test plate is not perpendicular to the optic. The actual path (exaggerated) is represented by the dotted line. Left: Magnified view of the air gap between the test plate and facesheet.

Cause	Effect, ΔR	Comments
Inaccurately measuring the gap, ΔR_{gap}	Δd	Good tools can measure distance to 5 microns.
Not removing all of the power, ΔR_{power}	$-8 (R/\#)^2 \Delta S$	$\Delta R_{\text{power}} = \frac{\lambda}{20}$ is normal.
The “cosine” effect, ΔR_{cos}	$-8 (R/\#)^2 d \cdot \alpha^2$	Minimize this error by making d small.

Table 1. Sources for error in the radius measurement, ΔR . The R-number ($R/\#$) is the segment ROC over the diameter, $\frac{R}{D}$. ΔS is the residual power (or sag), α is the slope error (deviation from normal incidence), and d is the distance between the test plate and facesheet.

30.3 μm . As with all RSS calculations, the largest value has the biggest effect on the overall result. For this situation, ΔR_{power} will drive the final number.

Error	Amount (μm)	Contributing Parameters
ΔR_{gap}	5	We can measure the gap to 5 μm
ΔR_{power}	-25.3	F/5 segment with $\frac{\lambda}{20}$ of residual power
ΔR_{cos}	-16	2 cm gap and 0.001 radian slope error
RSS:	30.3	

Table 2. Results for a typical example. The ΔR_{power} is the driving factor in this calculation.

APPENDIX A. DERIVATION: RELATIONSHIP BETWEEN WAVEFRONT VARIANCE AND COEFFICIENT W_{20}

We begin with the expression for variance:

$$\begin{aligned}\sigma^2 &= \overline{\Delta W^2} - (\overline{\Delta W})^2, \\ &= \left[\frac{1}{\pi} \int_0^{2\pi} \int_0^1 \Delta W^2(\rho, \theta) \rho \, d\rho \, d\theta \right] - \frac{1}{\pi^2} \left[\int_0^{2\pi} \int_0^1 \Delta W(\rho, \theta) \rho \, d\rho \, d\theta \right]^2.\end{aligned}$$

For defocus, $\Delta W = W_{20}\rho^2$. We'll make this substitution and continue as follows:

$$\begin{aligned}\sigma^2 &= \left[\frac{1}{\pi} \int_0^{2\pi} \int_0^1 (W_{20}\rho^2)^2 \rho \, d\rho \, d\theta \right] - \frac{1}{\pi^2} \left[\int_0^{2\pi} \int_0^1 W_{20}\rho^2 \rho \, d\rho \, d\theta \right]^2, \\ &= \frac{W_{20}^2}{3} - \frac{W_{20}^2}{4}, \\ &= \frac{W_{20}^2}{12}.\end{aligned}$$

Finally, we'll take a square root to solve for σ :

$$\begin{aligned}\sigma &= \frac{W_{20}}{\sqrt{12}}, \\ &= 0.289 W_{20}\end{aligned}$$

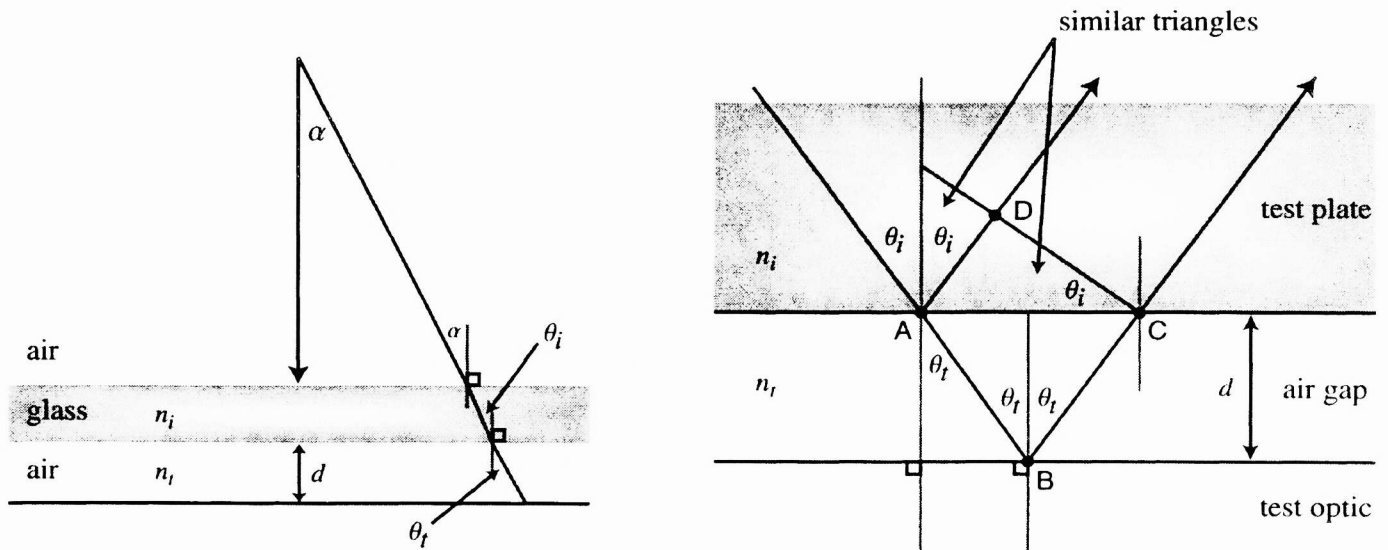


Figure 8. Geometry of the path difference derivation. Left: when light is at normal incidence, the path through the gap is $2d$. When light is incident at an angle α , the OPD is not $2d$. Right: closeup view of glass/air interface.

APPENDIX B. DERIVATION: THE “COSINE” EFFECT IN THE RADIUS MEASUREMENT

We now present the full derivation for Equation 7. As we mentioned in Section 3.2, when light is normal to the test glass, the optical path difference (OPD) is $2d$. When light is incident at an angle α , the OPD is different. We will derive the actual path difference and show the effect this has on the accuracy of the radius measurement. For simplicity, we will consider a plane parallel plate instead of a curved surface. We also assume that the two optics rest parallel with respect to each other. Figure 8 shows the geometry of the situation.

We'll start by writing down the OPD for the transmitted and reflected rays,

$$\text{OPD} = (\overline{AB} + \overline{BC}) - (n_i)\overline{AD}. \quad (8)$$

Note that \overline{AB} is equal to \overline{BC} because we assume that the test plate and test surface are parallel to each other. We can express \overline{AB} in terms of θ_t and the distance between the two optics, d :

$$\overline{AB} = \frac{d}{\cos \theta_t}. \quad (9)$$

We can now write Equation 8 as follows:

$$\text{OPD} = \frac{2d}{\cos \theta_t} - (n_i)\overline{AD}. \quad (10)$$

We know that \overline{AD} is related to θ_i by the following equation:

$$\sin \theta_i = \frac{\overline{AD}}{\overline{AC}}. \quad (11)$$

Finding \overline{AC} is a little tricky. We can use half of triangle $\triangle BAC$ to get the following relation:

$$\sin \theta_t = \frac{\frac{\overline{AC}}{2}}{\overline{AB}}.$$

We'll solve the above equation for \overline{AC} and replace \overline{AB} with the expression from Equation 9:

$$\begin{aligned}\overline{AC} &= 2\overline{AB} \sin \theta_t, \\ &= \frac{2d \sin \theta_t}{\cos \theta_t}, \\ &= 2d \tan \theta_t.\end{aligned}\tag{12}$$

We can now solve for \overline{AD} in Equation 11 using the expression for \overline{AC} in Equation 12:

$$\begin{aligned}\overline{AD} &= 2d \tan \theta_t \sin \theta_i, \\ &= 2d \tan \theta_t \frac{n_t}{n_i} \sin \theta_t,\end{aligned}\tag{13}$$

where we have used Snell's Law to replace $\sin \theta_i$ with $\frac{n_t}{n_i} \sin \theta_t$. Note that for this example, n_t is in air so it's equal to one.

We can finally complete our expression for the OPD between the two paths using Equations 10 and 13:

$$\begin{aligned}\text{OPD} &= \left(\frac{2d}{\cos \theta_t} \right) - n_i \left(2d \tan \theta_t \frac{1}{n_i} \sin \theta_t \right), \\ &= \frac{2d}{\cos \theta_t} (1 - \sin^2 \theta_t), \\ &= 2d \cos \theta_t.\end{aligned}\tag{14}$$

We can express the final equation in terms of the slope error, α :

$$\text{OPD} = 2d \cos \alpha.$$

Note that θ_t is equal to α and represents the angle between the incident ray and the surface normal. For normal incidence ($\alpha = 0$) this error is zero.

The error in the sag measurement is the difference in the two optical paths:

$$\begin{aligned}\Delta S &= \text{OPD}_\perp - \text{OPD}_\alpha, \\ &= 2d - 2d \cos \alpha \\ &= 2d (1 - \cos \alpha) \\ &\approx d \cdot \alpha^2\end{aligned}$$

Finally, we can use Equation 6 to find ΔR :

$$\Delta R_{\cos} = -8 (R/\#)^2 d \alpha^2.$$

REFERENCES

1. F. J. Cobos et. al., "The Hobby-Eberly telescope low resolution spectrograph: optical design," in *Optical Astronomical Instrumentation*, S. D'Odorico, ed., *Proc. SPIE* **3355**, pp. 424–432, 1998.
2. G. J. Hill et. al., "The Hobby-Eberly telescope low resolution spectrograph: mechanical design," in *Optical Astronomical Instrumentation*, S. D'Odorico, ed., *Proc. SPIE* **3355**, pp. 433–443, 1998.
3. J. E. Greivenkamp and J. H. Bruning, "Phase shifting interferometers," in *Optical Shop Testing, Second Ed.*, D. Malacara, ed., pp. 501–598, John Wiley & Sons, 1992.
4. J. H. Burge, "Efficient testing of off-axis aspheres with test plates and computer-generated holograms," in *Optical Manufacturing and Testing III*, H. P. Stahl, ed., *Proc. SPIE* **3782**, pp. 348–357, 1999.